

Single switch surface hopping for molecular dynamics with transitions

Clotilde Fermanian Kammerer^{1,a)} and Caroline Lasser^{2,b)}¹*Laboratoire d'Analyse et de Mathématiques Appliquées, UMR 8050, Université Paris Est, 94010 Créteil, France*²*Fachbereich Mathematik, Freie Universität Berlin, 14195 Berlin, Germany*

(Received 7 December 2007; accepted 4 February 2008; published online 8 April 2008)

A trajectory surface hopping algorithm is proposed, which stems from a mathematically rigorous analysis of propagation through conical intersections of potential energy surfaces. Since nonadiabatic transitions are only performed when a classical trajectory attains one of its local minimal surface gaps, the algorithm is called single switch surface hopping. Numerical experiments for a two mode Jahn–Teller system are presented, which illustrate the asymptotic justification of the method as well as its good performance in the physically relevant parameter range.

© 2008 American Institute of Physics. [DOI: [10.1063/1.2888549](https://doi.org/10.1063/1.2888549)]

I. INTRODUCTION

There are numerous dynamical processes in biology and chemistry for which nonadiabatic transitions have to be considered. Examples can be found in photoinduced or surface chemistry, just to mention two active areas of research. At the core of such processes is the violation of an adiabatic principle. The motion of the system's heavier constituents is not fully governed by a single averaged quantity of the lighter ones, since heavy and light particles interact in a more complicated way. Such nonadiabatic interactions occur if different averages coincide for certain configurations of the heavy particles. In the context of the Born–Oppenheimer approximation in quantum molecular dynamics, the heavy and light particles are the nuclei and the electrons, respectively, while the averages are the eigenvalues of the electronic Hamiltonian, which parametrically depend on the nuclear configuration.

The numerical simulation of nonadiabatic quantum dynamics poses several challenges. First, the underlying time-dependent Schrödinger equation is a partial differential equation, whose solution is highly oscillatory with respect to time and space. Hence, any attempt of directly computing the wave function faces the difficulty of properly resolving high-frequency oscillations. Second, the dimension of the position space is typically large. Depending on the system of interest, one might consider up to 20 or 30 degrees of freedom, which excludes a grid-based discretization approach. Third, the construction of the Schrödinger operator's potential is very difficult due to the high dimension. A first principles approach needs to determine the relevant electronic eigenvalues and eigenvectors for a sufficiently large set of nuclear configurations and to construct an appropriate diabatic potential matrix out of them. Often, one only obtains the eigenvalue surfaces, and the Schrödinger operator for the description of the nonadiabatic process is not even fully defined.

One of the most widely applied methods for simulating

nonadiabatic dynamics is trajectory surface hopping, which has been proposed first by Tully and Preston in 1971 (Ref. 1) with manifold developments since then.^{2–13} The basic idea is to combine classical transport on the eigenvalue surfaces with nonadiabatic hops between them. The way of nonadiabatic hopping distinguishes the variants of the method. The single switch algorithm we propose is motivated by the mathematical analysis of propagation through conical surface intersections using Wigner measures¹⁴ and Wigner functions.^{15,16} Each classical trajectory is subject to a deterministic branching process. The branching occurs whenever a trajectory attains one of its local minimal gaps between the eigenvalue surfaces. The new branches are weighed according to a multidimensional Landau–Zener formula for conical intersections.

Surface hopping is a genuine grid-free approximation method applicable for high-dimensional simulations. It allows one to compute quadratic quantities of the wave function such as energy surface populations or position and momentum expectation values with respect to the surfaces. Their direct numerical computation is advantageous, since their dynamics are less oscillatory than those of the wave function itself. The single switch method specifically requires classical transport and the identification of minimal surface gaps along trajectories. Hence, it need not resolve oscillations with respect to time but only space related oscillations when determining the initial phase space points for the classical transport.

The drawback of the nonoscillatory branching scheme is the possibly incorrect approximation of intersurface interferences. If there are classical trajectories on different surfaces, which arrive with comparable momenta simultaneously near a conical intersection point, then the simple Landau–Zener branching might be wrong, since it does not account for possible interferences between the surfaces during the transition process. However, the arrival of comparable trajectories near the intersection is only a necessary condition for the method's failure and not a sufficient one.¹⁷

The most prominent feature of single switch surface hopping is its asymptotic justification by a rigorous math-

^{a)}Electronic mail: clotilde.fermanian@univ-paris12.fr.^{b)}Electronic mail: lasser@math.fu-berlin.de.

emathical analysis. One can prove convergence to the true solution in the limit of a small semiclassical parameter h tending to zero.^{14–16} This parameter can be thought of as the square root of the inverse atomic mass. The proven convergence rate¹⁶ is of the order of $h^{1/8}$. However, all numerical experiments so far have even shown faster convergence^{16,18} with a rate of the order of $h^{1/2}$.

We proceed as follows. Section II states time-dependent Schrödinger systems with conical intersections, specifies the quantities to be computed, and formulates the single switch algorithm. The invariance of the multidimensional Landau–Zener formula with respect to different diabatic potentials as well as its relation to the formula employed by Voronin, *et al.*⁸ is discussed in Sec. III. Then, Sec. IV presents numerical experiments for a Jahn–Teller system with Gaussian initial data. Section V indicates an extension of the method to conical intersections of two twofold eigenvalues. Finally, Sec. VI summarizes our results.

II. ALGORITHM

Let

$$V(q) = \begin{pmatrix} v_{11}(q) & v_{12}(q) \\ v_{12}(q)^* & v_{22}(q) \end{pmatrix}$$

be a Hermitian matrix, whose entries depend smoothly on $q \in \mathbb{R}^d$. Schrödinger equations with real symmetric potential matrix $V(q)$ describe molecules, for which nuclear spin can be neglected and the number of electrons is even. Hermitian but not real symmetric matrices are used for systems with an external magnetic field.¹⁹

Let $\lambda^-(q) \leq \lambda^+(q)$ denote the eigenvalues of $V(q)$. We assume the following on their intersection set. If the matrix is real symmetric, then $\{q \in \mathbb{R}^d \mid \lambda^-(q) = \lambda^+(q)\}$ is a smooth submanifold of \mathbb{R}^d with codimension two. Otherwise, it is of codimension three. Roughly speaking, codimension two and three intersections are determined by two or three independent parameters. For codimension two crossings, there are two coordinates, such that near an intersection point the eigenvalue surfaces resemble two cones touching each other in their ends. Generally, there are coordinates such that the surfaces locally look like

$$\pm |y| = \begin{cases} \pm \sqrt{y_1^2 + y_2^2}, & \text{codim 2,} \\ \pm \sqrt{y_1^2 + y_2^2 + y_3^2}, & \text{codim 3.} \end{cases}$$

Therefore, one calls all such intersections conical.²⁰

We do not directly solve the Schrödinger equation

$$ih\partial_t\psi = -\frac{\hbar^2}{2}\Delta_q\psi + V\psi, \quad \psi(0) = \psi_0 \quad (1)$$

but compute particular quadratic quantities of its solution ψ . The first examples are the energy level populations, which give the probability that the wave function belongs to one of the two level spaces. If $\chi^\pm(q)$ denotes two normalized eigenvectors associated with $\lambda^\pm(q)$ and $\psi^\pm(q, t) := \langle \chi^\pm(q) \mid \psi(q, t) \rangle_{\mathbb{C}^2}$, then the level populations are given as

$$\langle \psi^\pm(t) \mid \psi^\pm(t) \rangle_{L^2} = \int_{\mathbb{R}^d} |\psi^\pm(q, t)|^2 dq.$$

We also aim at computing expectation values

$$\langle A\psi^\pm(t) \mid \psi^\pm(t) \rangle_{L^2} = \int_{\mathbb{R}^d} A\psi^\pm(q, t)\psi^\pm(q, t)^* dq$$

for observables $A = \text{op}(a)$, which stem from the Weyl quantization of smooth functions on classical phase space $a: \mathbb{R}^{2d} \rightarrow \mathbb{C}$, $(q, p) \leftrightarrow a(q, p)$. Examples are the position operator $\text{op}(a): \psi(q) \leftrightarrow q_j\psi(q)$ or the momentum operator $\text{op}(a): \psi(q) \leftrightarrow -ih\partial_j\psi(q)$ in the j direction, which are generated by the functions $a(q, p) = q_j$ and $a(q, p) = p_j$, respectively.

If one chooses a different pair of normalized eigenvectors $\tilde{\chi}^\pm(q)$, then the expectation values generally differ by a term of the order of h . Indeed, since the eigenspaces are one-dimensional, the eigenvectors are related by a gauge, that is, $\tilde{\chi}^\pm(q) = \exp(i\theta^\pm(q))\chi^\pm(q)$ with $\theta^\pm(q) \in \mathbb{R}$. Denoting the

corresponding scalar wave functions by $\tilde{\psi}^\pm(q, t) := \langle \tilde{\chi}^\pm(q) \mid \psi(q, t) \rangle_{\mathbb{C}^2}$, one obtains

$$\langle A\psi^\pm(t) \mid \psi^\pm(t) \rangle_{L^2} = \langle A\tilde{\psi}^\pm(t) \mid \tilde{\psi}^\pm(t) \rangle_{L^2} + O(h)$$

as $h \rightarrow 0$, where the $O(h)$ remainder term only arises for observables with p -dependent symbol $a(q, p)$ and depends on derivative bounds of the functions $\theta^\pm(q)$.

The crucial point is that quadratic quantities can be expressed as phase space integrals with respect to Wigner functions. For scalar wave functions $\psi: \mathbb{R}^d \rightarrow \mathbb{C}$, the Wigner function

$$(W\psi)(q, p) = (2\pi\hbar)^{-d} \int_{\mathbb{R}^d} e^{iyp/\hbar} \psi\left(q - \frac{1}{2}y\right) \psi\left(q + \frac{1}{2}y\right)^* dy$$

is a real-valued function on phase space, $W\psi: \mathbb{R}^{2d} \rightarrow \mathbb{R}$. It satisfies

$$\langle A\psi \mid \psi \rangle_{L^2} = \int_{\mathbb{R}^{2d}} a(q, p)(W\psi)(q, p) dq dp$$

for all Weyl-quantized operators $A = \text{op}(a)$. For the energy level populations, for example, one obtains

$$\langle \psi^\pm(t) \mid \psi^\pm(t) \rangle_{L^2} = \int_{\mathbb{R}^{2d}} (W\psi^\pm(t))(q, p) dq dp,$$

while the momentum expectation value in the j direction reads as

$$\langle -ih\partial_j\psi^\pm(t) \mid \psi^\pm(t) \rangle_{L^2} = \int_{\mathbb{R}^{2d}} p_j(W\psi^\pm(t))(q, p) dq dp.$$

This phase space point of view has motivated the mathematical analysis^{14–16} of Schrödinger equations with conical intersections, which, in turn, suggest the single switch surface hopping algorithm:

- (A) Sampling of the initial Wigner function;
- (B) classical transport of the sampling points;

- (C) branching of the trajectories, whenever they attain a local minimal eigenvalue gap, and weighing according to a generalized Landau–Zener formula; and
- (D) final computation of expectation values.

In the following, we provide the necessary details for the four constitutive steps of the algorithm. We describe the codimension three situation which can be easily simplified to the codimension two case.

A. Sampling

One samples the two initial Wigner functions $(q,p) \leftrightarrow (W\psi^\pm(0))(q,p)$ to obtain two sets of phase space points, the one related with the upper and the other with the lower surface. The choice of the normalized eigenvectors $\chi^\pm(q)$ defining $\psi^\pm(q,0)$ is not important, since their different phases just cause deviations of the order of h which are absorbed by the total error of the algorithm.

The initial sampling is the computational bottleneck of the algorithm. It requires the approximation of high-dimensional oscillatory Fourier integrals for determining the Wigner function in a large number of phase space points. The numerical experiments in Sec. IV focus on two-dimensional Gaussian initial data, such that the integrals are solved analytically and the subsequent sampling is based on a grid. In higher dimensions for general initial data, such an approach is not feasible, and one has to rely on Monte Carlo techniques. Moreover, the Wigner function of a non-Gaussian wave function attains negative values, which requires a suitable adaption of sampling strategies devised for positive functions.

B. Transport

The sample points and their associated real-valued weight are transported along the trajectories of the corresponding Hamiltonian systems $\dot{q}=p$, $\dot{p}=-\nabla_q \lambda^\pm(q)$.

C. Transitions

One monitors, when a trajectory (q_t, p_t) attains a local minimum along the surface gap $g(q)=\lambda^+(q)-\lambda^-(q)$, that is, when the function $t \leftrightarrow g(q_t)$ attains a local minimum. Discussing the gap condition more thoroughly, we write the potential matrix as the sum of half its trace and its trace-free part, that is,

$$V(q) = \frac{1}{2} \text{tr}(V(q)) + \begin{pmatrix} v_1 & v_2 + iv_3 \\ v_2 - iv_3 & -v_1 \end{pmatrix},$$

where $v(q)=(v_1(q), v_2(q), v_3(q))$ is a vector in \mathbb{R}^3 . Since the gap can be expressed as

$$g(q) = 2\sqrt{v_1(q)^2 + v_2(q)^2 + v_3(q)^2} = 2|v(q)|,$$

a sufficient condition for a trajectory attaining a local minimal gap at a point (q,p) is

$$\langle dv(q)p|v(q) \rangle_{\mathbb{R}^3} = 0, \quad (2)$$

where $dv(q)$ denotes the $3 \times d$ gradient matrix of $v(q)$. At points (q,p) with local minimal gap, all trajectories split.

The new branch starts on the other surface at the same point (q,p) and has the old weight times a Landau–Zener factor

$$T(q,p) = \exp\left(-\frac{\pi}{h} \frac{|v(q)|^2}{|dv(q)p|}\right). \quad (3)$$

The branch remaining on the same surface is reweighed by the factor of $1-T(q,p)$. Assuming that $|dv(q)p|$ is of the order of one with respect to the small parameter h , the Landau–Zener rate only causes a significant contribution, when the gap $g(q)=2|v(q)|$ is of the order of $h^{1/2}$. Hence, one can tighten the branching condition by additionally requiring that the gap is of the order of $h^{1/2}$, i.e.,

$$g(q) = O(h^{1/2}), \quad (4)$$

which, in turn, reduces the number of trajectories and does not affect the transition rate.

D. Final computation

At some final time t , one obtains two sets of phase space points, the one associated with the lower surface, and the other with the upper surface. Each point carries its specific weight, depending on how many transitions the trajectory has experienced and where in phase space they have occurred. If N points $(q_1, p_1), \dots, (q_N, p_N)$ with associated weights w_1, \dots, w_N have arrived on the upper surface, for example, then any expectation value can be approximated as

$$\begin{aligned} \langle A\psi^\pm(t)|\psi^\pm(t) \rangle_{L^2} &= \int_{\mathbb{R}^{2d}} a(q,p)W(\psi^\pm(t))(q,p)dqdp \\ &\approx \sum_{j=1}^N a(q_j, p_j)w_j\delta_j, \end{aligned}$$

where $\delta_j \geq 0$ denotes a suitable weight for numerical integration. In the case of a grid-based initial sampling, the integration weight might be the volume element of the corresponding initial point. For a Monte Carlo sampling, the weight might be $1/N$.

III. LANDAU–ZENER FORMULA

Since diabatic potentials are not uniquely defined, we address the dependence of the single switch algorithm on the choice of a diabatic potential. Let us suppose that the potential matrices $V_1(q)$ and $V_2(q)$ have the same eigenvalues $\lambda^\pm(q)$. We denote by $\chi_{(1)}^\pm(q)$ and $\chi_{(2)}^\pm(q)$ normalized eigenvector pairs of the two matrices. Our aim is to compare the outcome of the algorithm, if two scalar wave functions $\psi_0^\pm: \mathbb{R}^d \rightarrow \mathbb{C}$ are given, and the initial data of the Schrödinger equation (1) with potential $V=V_j$ are chosen as $\psi_0 = \psi_0^+ \chi_{(j)}^+ + \psi_0^- \chi_{(j)}^-$ for $j=1,2$, respectively. Since the eigenvalues and their gap are the same, the classical transport and the points for nonadiabatic transitions are identical for both potentials, too. However, the Landau–Zener rates are different.

The trace-free part of the two matrices is determined by two vectors $v_{(1)}(q)$ and $v_{(2)}(q)$ in \mathbb{R}^3 . The corresponding rates read as

$$T_j(q,p) = \exp\left(-\frac{\pi}{h} \frac{|v_{(j)}(q)|^2}{|dv_{(j)}(q)p|}\right), \quad j = 1, 2.$$

Since the gap is $g(q) = 2|v_{(1)}(q)| = 2|v_{(2)}(q)|$, one only has to compare the terms $|dv_{(1)}(q)p|$ and $|dv_{(2)}(q)p|$. The intersection set is a smooth submanifold, which can be written as $\{q \in \mathbb{R}^d | v_{(j)}(q) = 0\}$. Hence, there exists an orthogonal matrix $P(q)$, which smoothly depends on q and satisfies $v_{(1)}(q) = P(q)v_{(2)}(q)$. Observing that for points (q,p) with $|v_{(1)} \times(q)|, |v_{(2)}(q)| = O(h^{1/2})$

$$dv_{(1)}(q)p = P(q)dv_{(2)}(q)p + O(h^{1/2}),$$

we obtain

$$T_1(q,p) = T_2(q,p) + O(h^{1/2}). \quad (5)$$

Thus, the difference between the transition rates is absorbed by the overall error of the algorithm.

Voronin *et al.* have adapted the original surface hopping algorithm of Tully and Preston, which assumes an avoided crossing situation, to conical intersections.⁸ They have proposed nonadiabatic transitions whenever a classical trajectory (q_t, p_t) attains a minimal surface gap in a point (q, p) at time τ . The parameters A and B of their Landau–Zener rate

$$T_* = \exp\left(-\frac{\pi 2A^2}{h B|p|}\right),$$

are determined from evaluating the formula

$$g(q_t) = \sqrt{(t - \tau)^2 B^2 |p|^2 + 4A^2}$$

at the three last points of time t . Then, they generate a random number ξ and perform a hop to the other surface if $T_* \geq \xi$. Otherwise, the trajectory continues on the same surface. The Landau–Zener rates T_* and $T(q,p)$ are closely related. Taylor expanding

$$v(q_t) = v(q) + (t - \tau)dv(q)p + O((t - \tau)^2),$$

the orthogonality condition [Eq. (2)] and the smallness of the gap $g(q) = 2|v(q)| = O(h^{1/2})$ yield

$$|v(q_t)|^2 = |v(q)|^2 + (t - \tau)^2 |dv(q)p|^2 + O(h^{1/2}),$$

and, consequently,

$$g(q_t) = \sqrt{4(t - \tau)^2 |dv(q)p|^2 + 4|v(q)|^2} + O(h^{1/2}).$$

Hence, the parameters A and B satisfy

$$(A, B) = (|v(q)|, 2|dv(q)p|/|p|) + O(h^{1/2}),$$

and the two Landau–Zener rates coincide up to a negligible term of the order of $h^{1/2}$. That is,

$$T_* = T(q,p) + O(h^{1/2}). \quad (6)$$

IV. NUMERICS

Our numerical experiments work with the Schrödinger equation for a linear $E \otimes e$ Jahn–Teller Hamiltonian²⁰ of the form

$$ih\partial_t \psi = -\frac{h^2}{2} \Delta_q \psi + \gamma |q|^2 \psi + \begin{pmatrix} q_1 & q_2 \\ q_2 & -q_1 \end{pmatrix} \psi, \quad \psi(0) = \psi_0,$$

where the strength of quadratic confinement is chosen as $\gamma = 3$. The initial data are products of a Gaussian wave packet centered at position q_0 and momentum p_0 with a normalized eigenfunction associated with the upper surface. That is, $\psi_0(q) = \psi_0^+(q)\chi^+(q)$ with

$$\psi_0^+(q) = \frac{1}{\sqrt{\pi h}} \exp\left(-\frac{1}{2h}|q - q_0|^2 + \frac{i}{h}\langle p_0, q - q_0 \rangle_{\mathbb{R}^2}\right) \quad (7)$$

and $\chi^+(q) = (\cos \theta_q, \sin \theta_q)$, where $\theta_q \in [-\pi/2, \pi/2[$ is half the polar angle of q .

Since one series of experiments varies the semiclassical parameter, the position center of the Gaussian is chosen in an h -dependent way,

$$q_0 = (5h^{1/2}, 0.5h^{1/2}),$$

$$h = 0.001, 0.005, 0.01, 0.05, 0.1,$$

such that the initial wave function is localized close to but with negligible overlap with the conical intersection point $(0,0)$. Jahn–Teller Hamiltonians for silver, copper, sodium, and potassium fitted by recent electronic structure calculations²¹ have associated semiclassical parameter $h = 0.005, 0.007, 0.011$, and 0.008 and quadratic confinement $\gamma = 2.613, 5.097, 0.524$, and 0.260 , respectively. These results motivate the range of values for h we have considered and the choice $\gamma = 3$. The momentum center is set as

$$p_0 = (-k, 0), \quad k = 0, 0.5, 1, 2, 3,$$

such that in the second series of experiments the wave function arrives at the intersection with different strength of momentum. The length of the time-interval $[0, t_f]$ with endpoint

$$t_f = \begin{cases} \pi(2\gamma)^{-1/2} & \text{for } h = 0.001, \\ \frac{5}{3} \pi(2\gamma)^{-1/2} & \text{otherwise,} \end{cases}$$

allows the wave function to pass the intersection two to three times in all our experiments.

The single switch algorithm is realized by a grid-based initial sampling. The initial Wigner functions are

$$(W\psi_0^+)(q,p) = (\pi h)^{-2} \exp\left(-\frac{1}{h}|q - q_0|^2 - \frac{1}{h}|p - p_0|^2\right)$$

and $(W\psi_0^-)(q,p) = 0$. Hence, there are no initial sampling points for the lower surface. The Wigner function for the upper surface is discretized on the four-dimensional rectangle $[(q_0, p_0) - 5h^{1/2}, (q_0, p_0) + 5h^{1/2}]$ with $m = 16$ uniformly distributed grid points per direction. Then, the minimal number N of phase space points $(q_1, p_1), \dots, (q_N, p_N)$ is determined such that

$$\sum_{j=1}^N (W\psi_0^+)(q_j, p_j) \delta_j \geq 1 - \frac{1}{10}h,$$

where $\delta_j = (10/m\sqrt{h})^4$. The classical transport equations are solved by the explicit Runge Kutta (4,5) method DOPRI45.

TABLE I. The differences in L^2 -norm of the solution computed by the Strang splitting scheme with full and half resolution. Each entry shows the maximum error of the eleven recorded points of time. All of them are below 10^{-4} .

h	0.001	0.005	0.01	0.05	0.1
Accuracy ($\times 10^4$)	0.10	0.12	0.09	0.07	0.07
k	0	0.5	1	2	3
Accuracy ($\times 10^4$)	0.11	0.09	0.09	0.17	0.60

Validating the results, we compare with level populations and expectation values obtained by a numerically converged Strang splitting scheme with 10^4 time steps, which uses the fast Fourier transform for discretizing the Laplacian by a 2048×1024 grid for $h=0.001$ and a 1024×512 grid otherwise. The second dimension is treated by half the number of grid points, since the initial data are mostly transported along the first position coordinate such that a computational domain of size $[a, b] \times [-(1/4)(b-a), 1/4(b-a)]$ with

$$[a, b] = \begin{cases} [-28h^{1/2}, 14h^{1/2}] & \text{for } h = 0.001, \\ [-18h^{1/2}, 18h^{1/2}] & \text{otherwise,} \end{cases}$$

is sufficient. Indeed, Table I shows that the solution computed with half the number of grid points per direction and half the number of time steps differs from the one with finer discretization by less than 10^{-4} . For more details of the implementation and related results for a model of retinal in rhodopsin, we refer to our previous publications.^{16,18}

A. Time dependence

The semiclassical parameter and the initial momentum are set to $h=0.01$ and $p_0=(-1, 0)$. Figure 1 shows the absolute error of the upper level population together with the absolute error of position and momentum expectation value along the first coordinate. That is, the plot illustrates the differences of $\langle \psi^+(t) | \psi^+(t) \rangle_{L^2}$, $\langle q_1 \psi^+(t) | \psi^+(t) \rangle_{L^2}$, and $\langle -ih \partial_1 \psi^+(t) | \psi^+(t) \rangle_{L^2}$ as computed by the splitting method

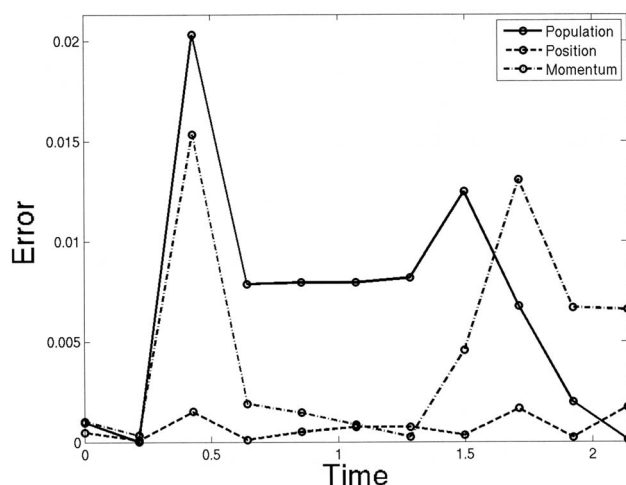


FIG. 1. Absolute error of population, position, and momentum expectation along the first coordinate as a function of time, all of them associated with the upper surface. The reference solution is computed by a numerically converged splitting scheme. All errors stay below 3%.

and the single switch algorithm as a function of time t . All errors stay below 3%, while those of the position expectation even remain in the promille range. There are pronounced peaks in the evolution of the three errors. A first simultaneous peak is around time $t=0.4$, while the second one occurs for the population error around $t=1.5$ and for the expectation values around $t=1.7$. These outliers correspond to changes in the upper level population down to 27, 15, and finally, up to 74%, as depicted in Fig. 2. Hence, significant parts of the wave function visit the intersection thrice, and the single switch algorithm resolves this dynamical effect with agreeable accuracy. Moreover, the errors' peaks also illustrate the effective character of the approximation. Based on a branching scheme combined with a generalized Landau-Zener formula to account for nonadiabatic transitions, it does only provide a coarse approximation of the dynamics very close to the intersection point but correctly describes the outgoing behavior of the wave function when it has passed by. The errors do not build up after having touched the intersection but decrease and remain stable.

The three visits of the wave function near the intersection are also reflected by the number of trajectories used by the single switch algorithm. Figure 3 shows jumps from roughly 2000 to 4000, 6000, and 9000 trajectories at those points of time, where the population changes significantly and the error peaks. The histogram of the nonadiabatic transition rates, which have occurred during the run of the algorithm, is u shaped. There are roughly 1100 trajectories with

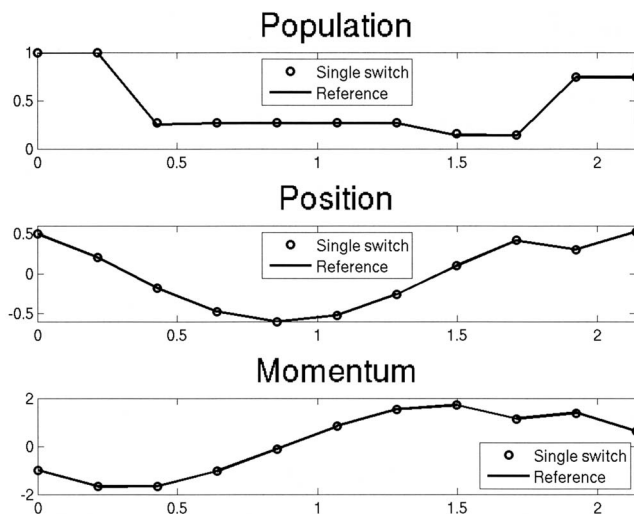


FIG. 2. Population, position, and momentum expectation along the first coordinate as a function of time, all of them associated with the upper energy surface. The results of the single switch algorithm follow the values of the reference solution. The plots correspond to the errors shown in Fig. 1.

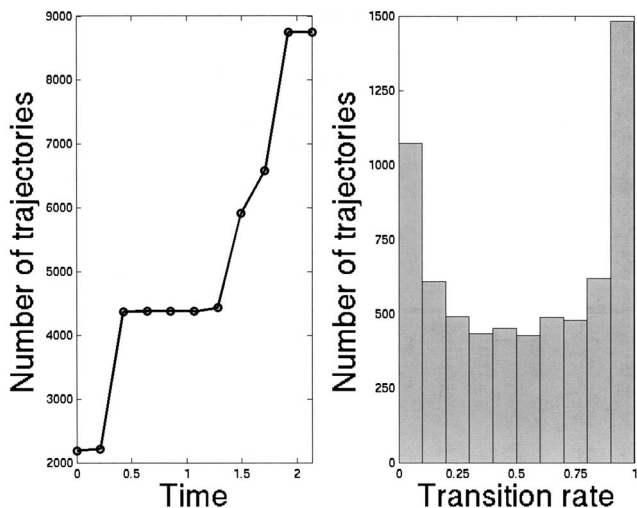


FIG. 3. Number of trajectories used by the single switch algorithm as a function of time. The histogram of the nonadiabatic transition rates shows maxima for small and large values of the rate. The arithmetic mean is 0.53.

associated transition rate below 0.1 and roughly 1500 with rate larger than 0.9. The arithmetic mean of the rates is 0.53.

B. Dependence on the semiclassical parameter

The initial momentum is set to $p_0=(-1,0)$, while the semiclassical parameter takes the values $h=0.001, 0.005, 0.01, 0.05$, and 0.1 . The plots in Fig. 4 show the time evolution of the lower surface population for the three intermediate choices of h . Again, the single switch algorithm follows the reference solution, which considerably changes surface population three times. Around time $t=0.4$, the lower surface population goes up by more than 50%, increases by roughly 10% around $t=1.5$, and drops by more than 50% after $t=1.7$.

Figure 5 presents the errors for the population, the position, and momentum expectation value along the first coordinate, and the energy expectation value as a function of the

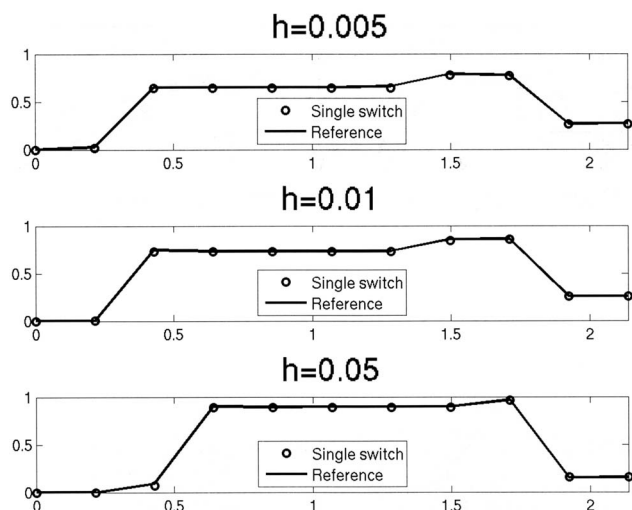


FIG. 4. Population of the lower surface as a function of time for $h=0.005, 0.01$, and 0.05 . As in Fig. 2, the population changes three times, the first and the last time by more than 50%, in between by roughly 10%.

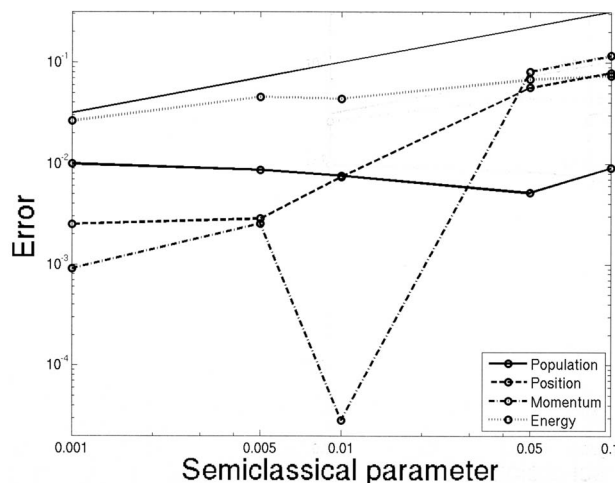


FIG. 5. Errors of mean population, position, and momentum expectation value along the first coordinate, and energy expectation value as a function of the semiclassical parameter, all of them related with the lower surface. The fine solid line is the function $h \rightarrow \sqrt{h}$.

semiclassical parameter, all of them related to the lower surface. The plot uses a double logarithmic scale. For each fixed value of h , the corresponding function value is the error of the arithmetic mean with respect to the 11 points of time the dynamics have been recorded at. Consequently, the mean energy expectation value is

$$\frac{1}{11} \sum_{j=1}^{11} \left\langle \left(-\frac{\hbar^2}{2} \Delta_q + \gamma |q|^2 - |q| \right) \psi^-(t_j) | \psi^-(t_j) \right\rangle_{L^2}.$$

The energy error is relative, while the other ones are absolute. As in our previous numerical experiments,^{16,18} all errors are bounded by the function $h \rightarrow \sqrt{h}$, which supports the mathematical justification of the single switch algorithm as an asymptotically correct method.

C. Dependence on initial momentum

The semiclassical parameter is set to $h=0.01$, while the initial momentum is $p_0=(-k,0)$ with $k=0, 0.5, 1, 2$, and 3 . The plot in Fig. 6 shows the absolute error of the population, the position, and momentum expectation values along the first coordinate, and the relative error of the energy expectation value as a function of the initial momentum component k . For each value of k , the corresponding function value is the error of the arithmetic means with respect to the recorded 11 points of time. The errors for the upper surface are roughly below 2%, while those for lower surface go up to roughly 5%. As in Fig. 5, the energy errors are the worst ones. This might be due to the coarse initial sampling, which approximates the initial energy only up to 2% (see Table II).

In the range $k \geq 1$, all but the curve for the lower surface energy are rather flat, while for small initial momentum the accuracy slightly deteriorates. One might be tempted to explain this tendency by the failure of the Landau-Zener rate $T(q,p)=\exp(-\pi/\hbar \cdot |q|^2/|p|)$ for vanishing momentum $p=0$. However, the histograms in Fig. 7 show, that all involved trajectories have nonzero momentum when arriving at their minimal surface gap and initiating a nonadiabatic branching.

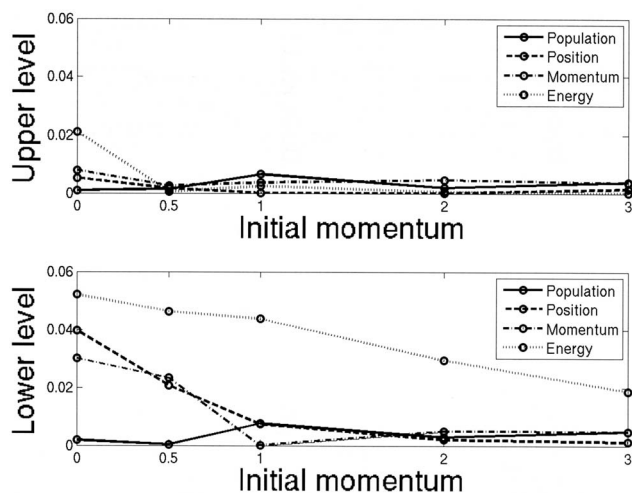


FIG. 6. Absolute errors of mean population, position, and momentum expectation along the first coordinate and relative error of mean energy expectation as a function of the initial momentum. All errors are roughly below 5%.

Figures 8 and 9 contain time-resolved plots of the population, the momentum expectation value along the first coordinate, and the energy expectation value for initial momentum components $k=0$ and $k=3$, all of them associated with the upper surface. For zero momentum $k=0$, the single switch algorithm does not reflect the three major changes in energy, which accompany the wave function's visits at the intersection. However, the maximal deviation of 0.08 around the third nonadiabatic transfer at time $t=1.7$ is embedded into a mean error of 0.03. In the regime of higher energies introduced by choosing $k=3$, the accuracy of the approximation naturally improves. Still the energy expectation shows two outliers at times of strong nonadiabatic coupling, however, at a smaller scale than before. The maximum deviation is 0.03 around the first nonadiabatic transition at $t=0.2$, while the mean error amounts to 0.007.

V. TWOFOLD EIGENVALUES

The single switch algorithm also extends to a class of Schrödinger equations, whose potential $V(q)$ has two twofold eigenvalues $\lambda^\pm(q)$ intersecting on a codimension 3 submanifold of \mathbb{R}^d . These potentials constitute the second type of codimension three crossings in Hagedorn's classification.²² Let us suppose that the trace-free part of the potential V is of the form

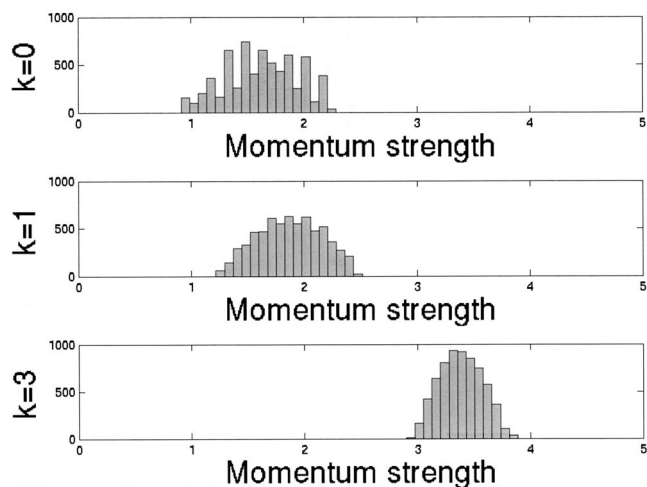


FIG. 7. Histogram of the trajectories' momenta when performing a nonadiabatic transition for initial momentum strength $k=0, 1$, and 3 . The corresponding arithmetic means are 1.63, 1.87, and 3.39, respectively.

$$B(v) = \begin{pmatrix} \begin{pmatrix} v_1 & v_2 + iv_3 \\ v_2 - iv_3 & -v_1 \end{pmatrix} & 0 \\ 0 & \begin{pmatrix} v_1 & v_2 - iv_3 \\ v_2 + iv_3 & -v_1 \end{pmatrix} \end{pmatrix}.$$

We denote by $\Pi^\pm(q) = \frac{1}{2}(\text{Id} \pm |v(q)|^{-1}B(v(q)))$ the two orthogonal matrices, which project on the two-dimensional eigenspaces. If one aims at computing expectation values for observables $B = \text{op}(b)$, whose symbol $b: \mathbb{R}^{2d} \rightarrow \mathbb{C}^{4 \times 4}$ is a scalar multiple of an eigenprojector, that is, $b(q, p) = a(q, p)\Pi^\pm(q)$ with $a: \mathbb{R}^{2d} \rightarrow \mathbb{C}$, then the algorithm stays the same. Examples are $b(q, p) = q_j \Pi^\pm(q)$ and $b(q, p) = p_j \Pi^\pm(q)$, which give the position and momentum expectation values in the j direction with respect to the level functions $\psi^\pm(q, t) := \Pi^\pm(q)\psi(t)$.

For resolving effects caused by the degeneracy of the eigenvalues, one needs observables $B = \text{op}(b)$, whose symbol satisfies $b(q, p) = \Pi^\pm(q)b(q, p)\Pi^\pm(q)$. They map into the largest class of matrices, which commute with the potential $V(q)$. If $\chi(q)$ is an eigenvector of $V(q)$, then the observable associated with $b(q) = \chi(q) \otimes \chi(q)$ describes orientation in one specific direction of one of the eigenspaces. In this more general situation, one has to modify the algorithm as follows:¹⁶

- (A) The initial sampling works with the two 4×4 matrices $\Pi^\pm(W\psi_0)\Pi^\pm$.
- (B) The classical transport is for $\dot{q} = p$, $\dot{p} = -\nabla_q \lambda^\pm(q)$.

TABLE II. Error of the initial sampling for the population, position and momentum energy expectation along the first coordinate, and the energy expectation with respect to the upper surface.

k	0	0.5	1	2	3
Population	0.001	0.001	0.001	0.001	0.001
Position	5×10^{-4}				
Momentum	2×10^{-5}	5×10^{-4}	10^{-3}	2×10^{-3}	3×10^{-3}
Energy	0.016	0.016	0.017	0.018	0.021

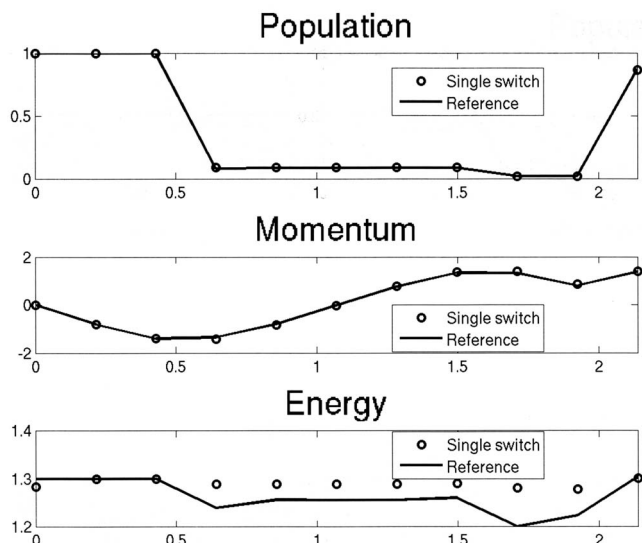


FIG. 8. Population, momentum expectation value along the first coordinate, and energy expectation value as a function of time, all of them related to the upper surface for initial momentum strength $k=0$. The mean energy error is 0.03.

- (C) The branching occurs, when a trajectory attains a local minimal gap with possibly condition (4), and the Landau–Zener rate is the same as in Eq. (3). However, for the branch remaining on the same surface the associated 4×4 matrix W is not only multiplied by $1 - T(q, p)$ but also conjugated by the matrix

$$\mathcal{R}(q, p) = \mathcal{B} \left(\frac{dv(q)p \wedge v(q)}{|dv(q)p \wedge v(q)|} \right), \quad (8)$$

where $x \wedge y = (x_2y_3 - x_3y_2, x_3y_1 - x_1y_3, x_1y_2 - x_2y_1)$ denotes the cross product between two vectors $x, y \in \mathbb{R}^3$. That is, the old and the new branch carry the weights $(1 - T(q, p))\mathcal{R}(q, p)W\mathcal{R}(q, p)$ and $T(q, p)W$, respectively.

- (D) The final expectation values are computed.

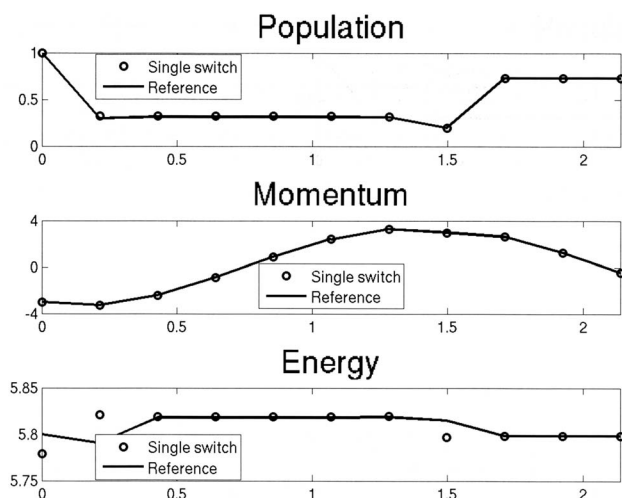


FIG. 9. Population, momentum expectation value along the first coordinate, and energy expectation value as a function of time, all of them related to the upper surface for initial momentum strength $k=3$. The mean energy error is 0.007.

The considerations of the previous Sec. III on the robustness of the method with respect to different diabatic potentials do not apply any more, since the matrix structure of the problem plays a crucial role.

VI. CONCLUSION

We have proposed a trajectory surface hopping algorithm for quantum propagation through conical intersections of energy surfaces. Since it is based on a branching scheme, which splits classical trajectories whenever they attain a local minimal surface gap, we have used the name *single switch surface hopping*. To our knowledge, the single switch algorithm is the first surface hopping algorithm with a rigorous mathematical derivation.

The original algorithm of Tully and Preston assumes an avoided crossing problem and allows for nonadiabatic hops when trajectories pass a precomputed avoided crossing seam. Among the many adaptations to conical intersections, the single switch method seems to be closest to the one of Voronin *et al.* Their and our approach assign each trajectory the same individual phase space points for nonadiabatic transfer and use equivalent Landau–Zener formulas [see relation (6)]. However, the branching of the single switch algorithm is deterministic, while the condition of Voronin *et al.* is probabilistic.

The single switch algorithm with hopping criteria [Eqs. (2) and (4)] is the realization of an asymptotic semigroup, which approximates the dynamics of the Wigner function with an error of the order of $\hbar^{1/8}$. Moreover, the algorithm is invariant with respect to different diabatic potentials.

The numerical experiments for a two mode Jahn–Teller system have focused on Gaussian wave packets as initial data, though the algorithm’s mathematical derivation allows for the general case. We have restricted ourselves to the simplest example of initial data, since an adequate initial sampling of less localized and more oscillatory wave functions poses a scientific challenge of its own. The simulations yield energy level populations, position, momentum, and energy expectation values with an accuracy of typically 2%. Experiments for a three mode Jahn–Teller-like model for pyrazine²³ have expectedly revealed the necessity to suppress trajectories with sufficiently small weight in order to keep the number of trajectories manageable. These results together with a systematic numerical comparison with other surface hopping algorithms will be discussed in a forthcoming publication.

ACKNOWLEDGMENTS

We thank P. Gérard and S. Teufel for their contribution to the works this article is based upon, and the referee for pointing us to the method of Voronin *et al.*

¹J. Tully and R. Preston, *J. Chem. Phys.* **55**, 562 (1971).

²W. Miller and T. George, *J. Chem. Phys.* **56**, 5637 (1972).

³N. Blais and D. Truhlar, *J. Chem. Phys.* **79**, 1334 (1983).

⁴G. Parlant and E. Gislason, *J. Chem. Phys.* **91**, 4416 (1989).

⁵J. Tully, *J. Chem. Phys.* **93**, 1061 (1990).

⁶B. Smith, M. Bearpark, M. Robb, F. Bernardi, and M. Olivucci, *Chem. Phys. Lett.* **242**, 27 (1995).

⁷O. Prezhdo and P. Rossky, *J. Chem. Phys.* **107**, 825 (1997).

- ⁸A. Voronin, J. Marques, and A. Varandas, *J. Phys. Chem. A* **102**, 6057 (1998).
- ⁹J. Fang and S. Hammes-Schiffer, *J. Phys. Chem. A* **103**, 9399 (1999).
- ¹⁰A. Jasper and D. Truhlar, *J. Chem. Phys.* **122**, 044101 (2005).
- ¹¹R. Spezia, I. Burghardt, and J. Hynes, *Mol. Phys.* **104**, 903 (2006).
- ¹²B. Levine and T. Martinez, *Annu. Rev. Phys. Chem.* **58**, 613 (2007).
- ¹³G. Granucci and M. Persico, *J. Chem. Phys.* **126**, 134114 (2007).
- ¹⁴C. Fermanian-Kammerer and P. Gérard, *Ann. Henri Poincaré* **4**, 513 (2003).
- ¹⁵C. Lasser and S. Teufel, *Commun. Pure Appl. Math.* **224**, 113 (2005).
- ¹⁶C. Fermanian-Kammerer and C. Lasser, "Propagation through generic level crossings: A surface hopping semigroup," *SIAM J. Math. Anal.* (to be published).
- ¹⁷C. Fermanian-Kammerer, *Math. Phys. Electron. J.* **13**, 4 (2007).
- ¹⁸C. Lasser, T. Swart, and S. Teufel, *Commun. Math. Sci.* **5**, 789 (2007).
- ¹⁹C. Mead, *J. Chem. Phys.* **70**, 2276 (1979).
- ²⁰*Conical Intersections*, edited by W. Domcke, D. Yarkony, and H. Köppel (World Scientific, Singapore, 2004).
- ²¹P. Garcia-Fernández, I. Bersuker, M. B. A. Aramburu, and M. Moreno, *Phys. Rev. B* **71**, 184117 (2005).
- ²²G. Hagedorn, *Mem. Am. Math. Soc.* **111** (1994).
- ²³R. Schneider and W. Domcke, *Chem. Phys. Lett.* **150**, 235 (1988).